



# Synchronous measurement and verification of position-independent geometric errors and position-dependent geometric errors in C-axis on mill-turn machine tools

Yu-Ta Chen<sup>1</sup> · Ting-Yu Lee<sup>2</sup> · Chien-Sheng Liu<sup>2</sup>

Received: 27 February 2022 / Accepted: 30 June 2022 / Published online: 13 July 2022  
© The Author(s), under exclusive licence to Springer-Verlag London Ltd., part of Springer Nature 2022

## Abstract

This paper proposes a synchronous measurement system of four position-independent geometric errors (PIGEs) and two position-dependent geometric errors (PDGEs) for the rotary axis in five-axis machine tools. The measuring instruments used in this system include a touch-trigger probe and two standard calibration spheres. The main contribution of this paper simultaneously and directly measures four PIGEs and two PDGEs (axial and angular positioning errors) through only one measuring process. It is expected to improve the deficiencies of previous studies measuring PIGEs and PDGEs separately. The geometric errors of the C-axis of a mill-turn machine tool MT-540 were analyzed. The calculation process includes the establishment of the mathematical model of the machine and geometric error equations. The least squares method was used to solve the linear overdetermined system and calculate the values of the geometric errors. Before solving the geometric errors, the accuracy of the calculation process was verified by using the simulated method. The simulation results also confirm the feasibility of this measurement system. Then the data obtained from the experiments were used to calculate the geometric errors of the machine tool. During the experiments, the calibration procedure of the touch-trigger probe was calibrated. After the calibration procedure was completed, the mechanical coordinate values of the two standard calibration balls were measured. The geometric error equations were programmed on a computer, and the data of calibration spheres obtained from the experimental measurements were substituted into the program to calculate the four PIGEs and two PDGEs.

**Keywords** Five-axis machine tool · Rotary axis · Geometric errors · Position-independent geometric errors · Position-dependent geometric errors · Touch-trigger probe · Mill-turn machine tool

## 1 Introduction

The demand for the use of five-axis computer numerical control (CNC) machine tools is increasing in recent years [1, 2]. Compared with conventional three-axis machine

tools, there are two rotary axes added in five-axis machine tools, and the movement mode with two more degrees of freedom increases the possibility of processing various curved surfaces [3, 4]. The five-axis machine tools also bring higher efficiency, automation, flexibility, and precision product processing strategy. To improve the accuracy requirements of five-axis machine tools, many manufacturers have turned their research directions to instruments and methods of measuring the rotary axis [5, 6]. Nowadays, the commercially available products commonly used to measure the geometric errors of the rotary axis of the machine tools are R-Test, QC20-W (Ballbar), XR20-W, LaserTRACER, AxiSet Check-Up, SWIVELCHECK, and so on. It is very important to improve the accuracy of the rotary axis. Therefore, this paper focuses on the measurement of the rotary axis of the five-axis machine tools. A touch-trigger probe was used in this paper because it has

✉ Chien-Sheng Liu  
cslu@mail.ncku.edu.tw

Yu-Ta Chen  
YuTaChen@stust.edu.tw

<sup>1</sup> Department of Mechanical Engineering, Yungkuang Dist., Southern Taiwan University of Science and Technology, No. 1, Nan-Tai Street, Tainan City 710301, Taiwan, Republic of China

<sup>2</sup> Department of Mechanical Engineering, National Cheng Kung University, Taiwan, No. 1, University Road, Tainan City 70101, Taiwan

the advantages of a low cost, a high accuracy, and simple and quick installation, when compared with the commercially available instruments [7, 8].

According to previous researches [9–11], the error sources that affect the machining accuracy of machine tools can be divided into three categories: static errors, dynamic errors, and quasi-static errors. Quasi-static errors include thermal errors and geometric errors. According to previous research [12], quasi-static errors accounted for 70% of all error sources. According to the research [13, 14], geometric errors themselves accounted for 30%. The geometric errors are a crucial factor affecting the accuracy of the machine tools. These all prove that solving the geometric errors can greatly improve the processing quality of the machine tools, and modern industries using automated machine tools require high-precision axes [15, 16]. The geometric errors of the rotary axis can be divided into two categories. One is the position independent geometric errors (PIGEs, also called location errors). There are 4 items of PIGEs. Another one is position-dependent geometric errors (PDGEs, also called component errors). There are 6 items of PDGEs. From previous researches [8, 17–19], it can be found that these researches only measured the PIGEs of the rotary axis, and other researches mainly analyzed the PDGEs of the rotary axis [20–22]. The PIGEs and the PDGEs affect the accuracy of the rotary axis of the machine tools at the same time, so this paper hopes to simultaneously consider the PDGEs and PIGEs. According to the literature [23, 24], angular positioning error is the most important among the 6 PDGEs of the rotary axis. The positioning accuracy of the rotary axis is an important indicator for evaluating the performance of the rotary axis. Therefore, the purpose of this paper is to simultaneously analyze the 4 PIGEs and 2 PDGEs (angular positioning and axial errors) of the rotary axis of the machine tools.

Jeong et al. used a touch-trigger probe to measure all the PIGEs of a four-axis machine tool. The research method used 2 standard calibration spheres and a touch-trigger probe to measure and used the height difference of the two spheres to obtain additional information to calculate the errors [25]. However, since the height of the calibration sphere in the calculation formula is an important piece of information, when the height measurement is inaccurate, it will greatly affect the measurement values of the PIGEs. Chen et al. used a touch-trigger probe with a standard calibration sphere to measure a five-axis machine tool and calculate a total of 8 PIGEs of dual-rotary axes [26]. The operation process is fast and requires only one calibration sphere, so the measurement efficiency is high, and the operation is simple and convenient. However, in its calculation process, the PDGEs of the rotary axis are not considered at the same time. Therefore, when the PDGEs are omitted

and only the PIGEs are considered, the error values will be slightly inaccurate.

To process a workpiece online and to measure its geometric information to calculate the geometric errors is another error measurement method. Ibaraki et al. [27], Li et al. [28] and Jiang et al. [29] have all proposed geometric error measurement methods by online machining a special-shaped workpiece on a machine, and the methods can include the impact of the thermal errors during machining the workpiece. However, machining the workpiece will increase many error causes, such as the influence of cutting force, which will decrease the accuracy of the original measurement target. Ibaraki also proposed other geometric shapes such as squares and used touch-trigger probes for geometric error measurement [8]. Ibaraki also proposed using special geometric shapes and rotating the rotary axis in different paths to measure different items of the geometric errors.

From the literature review, it can be found that the geometric error measurement methods mainly needed to use the spindle and the movement of each component to touch the standard part, or the machined workpiece to calculate the geometric errors. The difference between these researches is that the measured geometry and path were different. The purpose and contribution of the paper is to simultaneously analyze the 4 PIGEs and 2 PDGEs (angular positioning and axial errors) of the rotary axis of the machine tools.

## 2 System structure and measurement principle

### 2.1 Definition of geometric errors

Geometric errors can be divided into two categories [30, 31]. According to ISO230-1 [32] and ISO230-7 [33], geometric errors are defined as PIGEs and PDGEs. PIGEs are the offset when the assembly is inaccurate. These values are fixed and will not change with the movement of the axis. Due to the manufacturing deviation of components, each axis cannot move to the ideal position when it shifts. The ideal driving position given by the controller is not exactly equal to the actual moving position everywhere. This difference is the PDGEs.

There are two offset errors and two squareness errors in the PIGEs of a rotary axis. It means that the deviation of the ideal axis center and the actual axis center of the rotary axis has 4 degree-of-freedom errors. According to ISO230-7 [33], the PDGEs of the rotary axis are 6 degrees of freedom, which are 2 radial errors, 1 axial error, 2 tilt errors in two oblique directions, and 1 angular positioning error. This paper focuses on the synchronous measurement of the 4 PIGEs of the rotary axis and 2 PDGEs (angular positioning and axial errors) in rotary axis. Table 1 lists all geometric errors of the rotary axis and the red frame marks the focus of this paper.

**Table 1** All geometric errors of rotary axis of machine tools

Symbols used in this thesis		ISO	
<b>PIGEs (Rotary Axis)</b>	$O_{xc}$ (Linear offset error of C-axis in X direction)	<b>Location Errors (Rotary Axis)</b>	XOC
	$O_{yc}$ (Linear offset error of C-axis in Y direction)		YOC
	$S_{xc}$ (Squareness error of C-axis to Y-axis)		AOC
	$S_{yc}$ (Squareness error of C-axis to X-axis)		BOC
<b>PDGEs (Rotary Axis)</b>	$\delta_{xc}$ (Radial error)	<b>Component Errors (Rotary Axis)</b>	EXC
	$\delta_{yc}$ (Radial error)		EYC
	$C_{z(dep)}$ (Axial error)		EZC
	$\epsilon_{xc}$ (Tilt error)		EAC
	$\epsilon_{yc}$ (Tilt error)		EBC
	$C_{(pos)}$ (Angular positioning error)		ECC

### 2.2 Measured five-axis machine tool

As shown in Fig. 1, a mill-turn machine tool MT-540 (Yida Precision Machinery Co., Ltd.) was used in this paper. Its configuration belongs to the RTTTR configuration, which can also be called Table/Spindle-tilting Type and is a five-axis machine tool with BC axis. This machine tool can be used in lathe mode or converted to milling mode. Some products need to be processed by lathes and milling process. This kind of machine tool can complete all the processing procedures in one clamping and improve efficiency. Table 2 shows the specifications of the MT-540, and Fig. 2 is a schematic diagram of the position of each axis of the MT-540. The B-axis is also the spindle. For this paper, the touch-trigger probe was locked on the B-axis. The measured C-axis faces the left side of the machine. The main moving range of the spindle is near the C-axis worktable, so the stroke of the linear axes is also around this area. Compared with the

general machine tools, the strokes of the X, Y, and Z axes are quite short. The strokes of the X, Y, and Z axes are 660, 200, and 760 mm, respectively. Because the touch-trigger probe is translated via the linear axis, the short strokes cause the limited measurement range. This is an overcome problem in this paper.

### 2.3 Mounting of proposed measurement system

A Blum TC50 touch-trigger probe was used in this paper. Table 3 shows the specifications of the touch-trigger probe. Since the mill-turn machine tool used in this paper is a specific five-axis machine tool, the touch-trigger probe also needs a tool holder KM63 for connecting to the machine tools, as illustrated in Fig. 3. Due to the need of the measurement method, this paper requires two standard calibration spheres (two tungsten carbide spheres with a diameter of 18.999 mm) for measurement. As shown in Fig. 4, the

**Fig. 1** Mill-turn machine tool MT-540



two calibration spheres are attached to the worktable of the machine tool. However, as mentioned in Sect. 2.2, because the stroke of the linear axis is too small, it can only move around the *C*-axis table, resulting in the limited measurement range. Using the method shown in Fig. 4 will allow the *C*-axis to rotate at a severely limited angle. Therefore, the standard calibration spheres cannot be triggered by the probe when rotating a little angle, which affects the measurement process.

To solve the problem of the measurement range, a specific jig was designed. We considered the moving distance of the probe, locked the calibration spheres on the specific jig (see Fig. 5) and then attached it to the *C*-axis worktable.

**Table 2** MT-540 specifications

Type	MT-540	Unit
Tool holder	KM 63UT	
Stroke		
<i>B</i> -axis	$\pm 110^\circ/0.001^\circ$	Degrees
<i>C</i> -axis	$360^\circ/0.001^\circ$	Degrees
<i>X</i> -axis	660 (26.0")	mm (in.)
<i>Y</i> -axis	200 (7.87")	mm (in.)
<i>Z</i> -axis	760 (29.9")	mm (in.)
Machine size		
Length	4700 (185")	mm (inch)
Width	2800 (110.2")	mm (inch)
Height	2700 (106.3")	mm (inch)

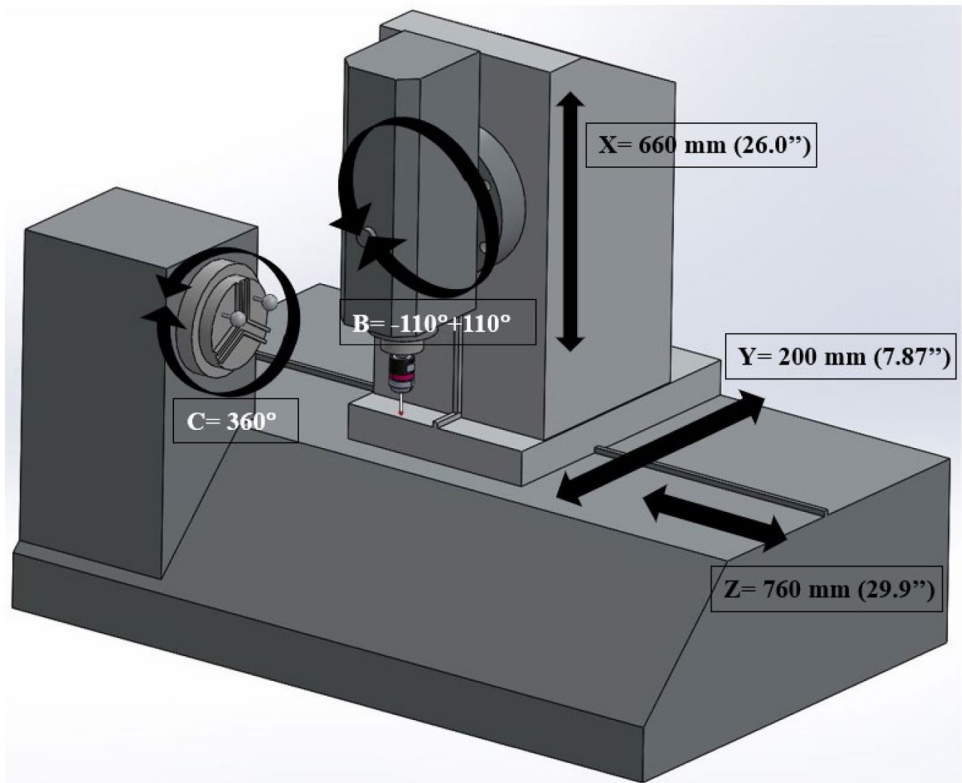
## 2.4 Measurement objectives and principle

As shown in Table 1, the measurement objectives of this paper are 4 PIGEs and 2 PDGEs (angular positioning and axial errors), analyzed simultaneously, and the red frame is the measurement target.

The measurement method of using the standard calibration spheres mainly needs quite accurate calibration spheres. This diameter of the standard calibration spheres can be used to calculate the values of the mechanical coordinate system of the center of the sphere in the machine tool. Five positions of the calibration sphere are touched to calculate the center coordinates of the sphere, as shown in Fig. 6. As shown in Fig. 7, when the calibration sphere is in the initial position, the *C*-axis rotates an angle. Due to the geometric errors of the *C*-axis, the axis of the *C*-axis is offset, resulting in a difference ( $dP$ ) between the ideal and the actual coordinates of the calibration sphere. With  $dP$ , the mathematical equations can be listed, and the geometric errors can be solved by mathematical methods.

The method of using the calibration sphere to establish the equations is shown in Fig. 8. As shown, the  $0^\circ$  of the *C*-axis is the first position, which is the starting measurement point. The gray ball is the point with no error in the first position. The blue circle is the path of the standard calibration sphere when there is no error in the ideal case. When the *C*-axis rotates, there will be black ball 2 position, black ball 3 position, black ball 4 position, and

**Fig. 2** Schematic diagram of MT-540



so on. After the *C*-axis rotates, there will be geometric errors. The method of establishing the *dP* equations, as shown in Table 4, will subtract the first ideal position from the second position, subtract the first ideal position from the third position, and subtract the first ideal position from the fourth position. After multiple sets of *dP* equations are listed, *dP* is used to analyze the error values.

**Table 3** Specifications of touch-trigger probe Blum TC50

Type	Blum TC50
Protection class	IP68
Approach direction	$\pm X, \pm Y, -Z$
Measuring force in <i>X</i> and <i>Y</i> directions	2 N
Measuring force in <i>Z</i> direction	7 N
Max deflection in <i>X</i> and <i>Y</i> directions	$\pm 15^\circ$
Max deflection in <i>Z</i> direction	10 mm
Max acceleration	50 m/s <sup>2</sup>
Repeatability	0.3 $\mu\text{m } 2\sigma$
Max probing speed	3 m/min
Mass	925 g
Signal transmission	Infrared
Range	$\pm 60^\circ$ in <i>Z</i> , $360^\circ$ in <i>X/Y</i>
Storage temperature	$-20^\circ\text{C} \dots +70^\circ\text{C}$
Operating temperature	$+5^\circ\text{C} \dots +50^\circ\text{C}$

### 3 Establishment of geometric error model

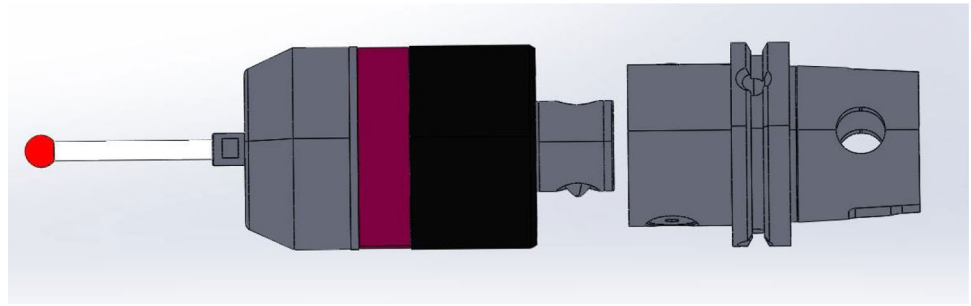
#### 3.1 Forward kinematics

The significance of forward kinematics is that after the forward kinematics is continuously multiplied by each matrix of the homogeneous transformation matrix, when the drive values of each axis, namely the servo commands  $x_{cmd}, y_{cmd}, z_{cmd}$  are known, the final pose matrix can be calculated by mathematical models. For machine tools, it is the coordinates of the touch-trigger probe relative to the reference coordinate system and the coordinates of the standard calibration spheres relative to the reference coordinate system. On the other hand, inverse kinematics is to push back the servo commands  $x_{cmd}, y_{cmd}, z_{cmd}$  of each axis when the pose matrix is known, as shown in Fig. 9.

The total components of the used machine tool are the *C*-axis (rotary axis), spindle (touch-trigger probe), *B*-axis (rotary axis), *X*-axis, *Y*-axis, and *Z*-axis. Our purpose is to find the relationship between the probe and the standard calibration spheres, so two kinematic chains, namely the probe kinematic chain and the calibration sphere kinematic chain, need to be constructed. From Fig. 2, the *C*-axis is a worktable, which is erected on the left side of the machine tool, and the standard calibration spheres are attracted to the end of the *C*-axis.

The kinematic chain of the touch-trigger probe: reference coordinate system  $R \rightarrow Z \rightarrow Y \rightarrow X \rightarrow B \rightarrow P$  (touch-trigger probe).

**Fig. 3** CAD model for connection between touch-trigger probe TC50 and KM63 tool holder



The standard calibration sphere kinematic chain: reference coordinate system  $R \rightarrow C \rightarrow S$  (standard calibration sphere). These two kinematic chains are used to find the correlation between the probe and the calibration sphere. Since the measurement object of this paper is the  $C$ -axis, the rotary  $B$ -axis does not rotate in this paper, and the geometric errors of  $B$ -axis is not considered here. The construction of forward kinematics first needs to use the homogeneous transformation matrix (HTM) to complete the error model.

When using the HTM to build a geometric error model for a machine tool, a coordinate system of each axis of the machine tool must be created. Figure 10 illustrates the coordinate system of each axis of the mill-turn machine tool, and then each coordinate system is connected into the two kinematic chains through the HTM. The HTM of the coordinate system of the  $C$ -axis relative to the reference coordinate system  $R$  is  ${}^R T_C$ , and  ${}^R T_C = T^{co} T^{cs} T^{c(dep)} T^c$ . Since the  $C$ -axis is the measured axis, the analyzed errors need to be put in the matrix.  $T^{co}$  is the offset

error matrix in the PIGEs of  $C$ -axis, and  $T^{cs}$  is the squareness error matrix in the PIGEs of the  $C$ -axis.  $T^{c(dep)}$  means the PDGEs of the  $C$ -axis, and  $T^c$  is the drive of the  $C$ -axis by the controller.  $\theta_c$  is the servo command value of the  $C$ -axis.  $O_{xc}$ ,  $O_{yc}$ ,  $S_{xc}$ , and  $S_{yc}$  are the 4 PIGEs of the  $C$ -axis.  $C_{z(dep)}$  and  $C_{(pos)}$  are the axial error and angular positioning errors, respectively, in the PDGEs of  $C$ -axis. The result of multiplying all error matrices is  ${}^R T_C$  as Eq. (1).

$$T^{co} = \begin{bmatrix} 1 & 0 & 0 & O_{xc} \\ 0 & 1 & 0 & O_{yc} \\ 0 & 0 & 1 & 0 \\ 0 & 0 & 0 & 1 \end{bmatrix} \quad T^{cs} = \begin{bmatrix} 1 & 0 & S_{yc} & 0 \\ 0 & 1 & -S_{xc} & 0 \\ -S_{yc} & S_{xc} & 1 & 0 \\ 0 & 0 & 0 & 1 \end{bmatrix} \quad T^{c(dep)} = \begin{bmatrix} 1 & 0 & 0 & 0 \\ 0 & 1 & 0 & 0 \\ 0 & 0 & 1 & C_{z(dep)} \\ 0 & 0 & 0 & 1 \end{bmatrix}$$

$$T^c = \begin{bmatrix} \cos(\theta_c + C_{(pos)}) & \sin(\theta_c + C_{(pos)}) & 0 & 0 \\ -\sin(\theta_c + C_{(pos)}) & \cos(\theta_c + C_{(pos)}) & 0 & 0 \\ 0 & 0 & 1 & 0 \\ 0 & 0 & 0 & 1 \end{bmatrix}$$

$${}^R T_C = \begin{bmatrix} \cos(\theta_c + C_{(pos)}) & \sin(\theta_c + C_{(pos)}) & S_{yc} & O_{xc} + C_{z(dep)} S_{yc} \\ -\sin(\theta_c + C_{(pos)}) & \cos(\theta_c + C_{(pos)}) & -S_{xc} & O_{yc} - C_{z(dep)} S_{xc} \\ -S_{yc} \cos(\theta_c + C_{(pos)}) - S_{xc} \sin(\theta_c + C_{(pos)}) & S_{xc} \cos(\theta_c + C_{(pos)}) - S_{yc} \sin(\theta_c + C_{(pos)}) & 1 & C_{z(dep)} \\ 0 & 0 & 0 & 1 \end{bmatrix} \quad (1)$$

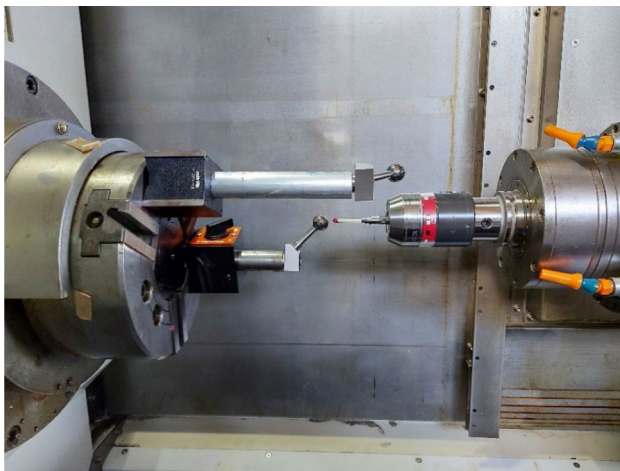


**Fig. 4** Experimental diagram using two standard calibration spheres

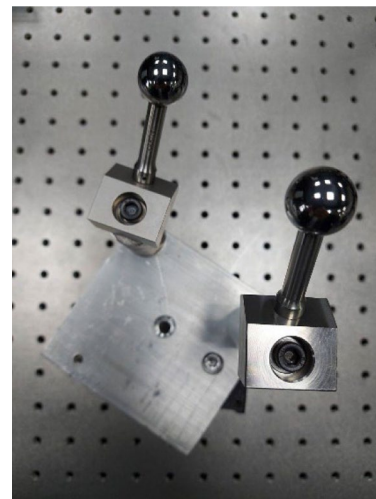


**Fig. 5** Jig with two calibration spheres

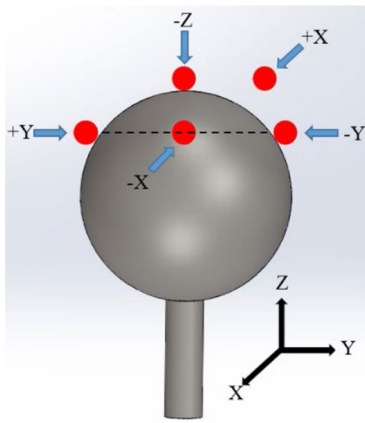


**Fig. 6** Measurement of center coordinates of the standard calibration sphere

${}^R T_Z, {}^Z T_Y, {}^Y T_X, {}^X T_B, {}^B T_P$  are the matrices in the kinematic chain of the touch-trigger probe, and  ${}^R T_C, {}^C T_S$  are the matrices in the kinematic chain of the standard calibration spheres. Then the HTM of probe coordinate system  $P$  relative to the reference coordinate system  $R$  and the HTM of the calibration sphere coordinate system  $S$  relative to the reference coordinate system  $R$  are constructed, respectively, as shown in Eqs. (2) and (3).

$${}^R T_P = {}^R T_Z {}^Z T_Y {}^Y T_X {}^X T_B {}^B T_P \tag{2}$$

$${}^R T_S = {}^R T_C {}^C T_S \tag{3}$$

### 3.2 Inverse kinematics

Section 3.1 introduces the touch-trigger probe kinematic chain and the standard calibration sphere kinematic chain in

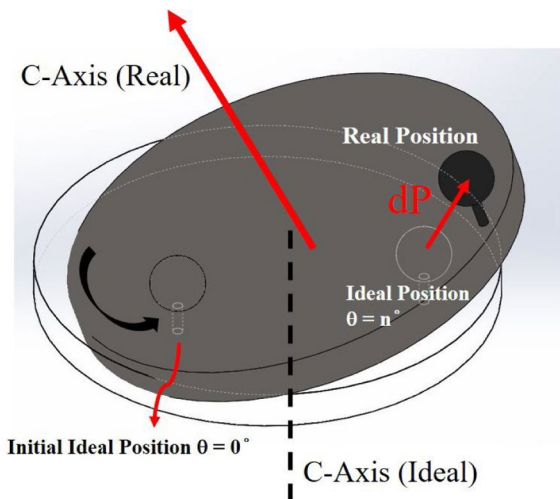


**Fig. 7** Difference between ideal and actual coordinates of calibration sphere

the mathematical model, respectively. For inverse kinematics, these two kinematic chains can be used to calculate the servo commands of the three linear axes. Because the touch-trigger probe will touch the standard calibration spheres, the values of the mechanical coordinate system of the spheres can be calculated. In other words, the two kinematic chains will collide with each other. Therefore, the coordinate values of the probe relative to the reference coordinate system and the calibration sphere relative to the reference coordinate system are the same, and the servo command can be calculated by using this feature.

The ideal servo command symbols are  $x_{cmd}^i, y_{cmd}^i,$  and  $z_{cmd}^i$  as Eqs. (4)–(6), respectively. The solved actual servo command symbols are  $x_{cmd}^r, y_{cmd}^r,$  and  $z_{cmd}^r$  as Eqs. (7)–(9), respectively. The solution results contain many quadratic terms, which mean that there are many errors' multiplied terms in the servo command equations, but the values of these terms are quite small. Therefore, Eqs. (7)–(9) are the simplified results after omitting the quadratic terms, and  $x_s, y_s,$  and  $z_s$  are the coordinates of the calibration sphere coordinate system ( $S$ ) relative to  $C$ -axis coordinate system.

$$x_{cmd}^i = x_s \cos(\theta_c) + y_s \sin(\theta_c) \tag{4}$$

$$y_{cmd}^i = y_s \cos(\theta_c) - x_s \sin(\theta_c) \tag{5}$$

$$z_{cmd}^i = -z_2 + z_s \tag{6}$$

$$x_{cmd}^r = O_{xc} + z_s S_{yc} + x_s \cos(\theta_c) + y_s C_{(pos)} \cos(\theta_c) + y_s \sin(\theta_c) - x_s C_{(pos)} \sin(\theta_c) \tag{7}$$

$$y_{cmd}^r = O_{yc} - z_s S_{xc} + y_s \cos(\theta_c) - x_s C_{(pos)} \cos(\theta_c) + x_s \sin(\theta_c) - y_s C_{(pos)} \sin(\theta_c) \tag{8}$$

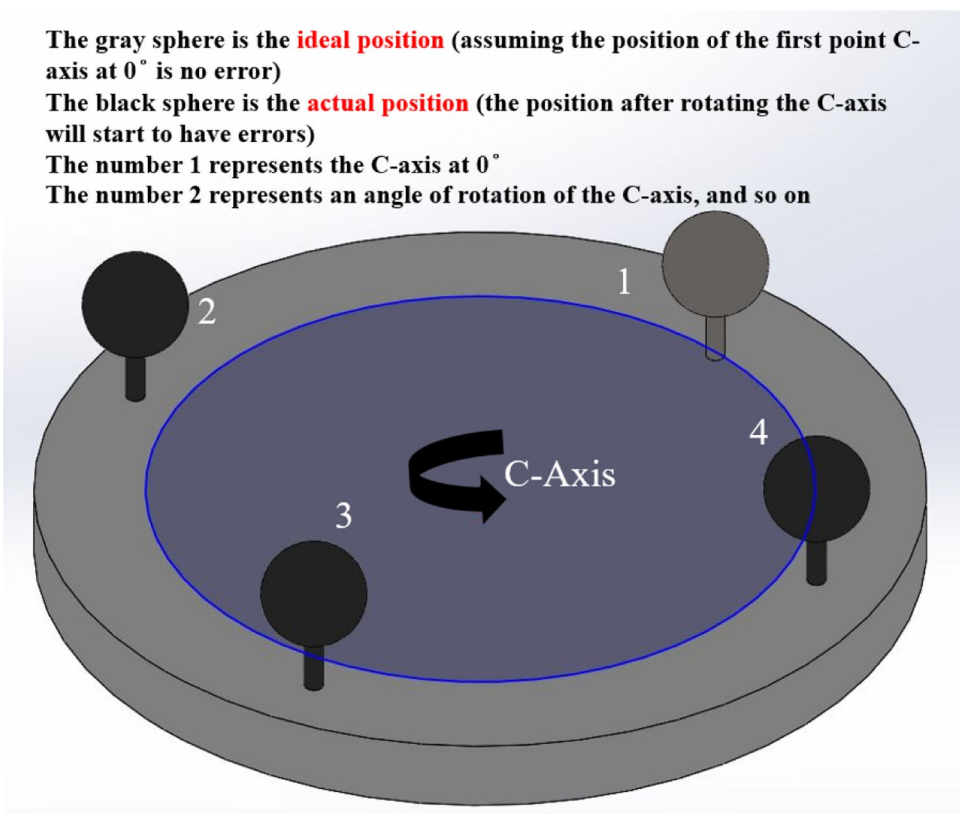
$$z_{cmd}^r = -z_2 + z_s + C_{z(dep)} + y_s S_{xc} \cos(\theta_c) - x_s S_{yc} \cos(\theta_c) - x_s S_{xc} \sin(\theta_c) - y_s S_{yc} \sin(\theta_c) \tag{9}$$

### 3.3 Assumptions of geometric error variables

There is a fundamental difference between PIGEs and PDGEs, as shown in Table 5. The values of PIGEs are the same in each angle of the rotary axis and will not change with the rotation of the rotary axis; the PDGEs are different when the rotary axis rotates at each angle. To analyze the key points of PIGEs and PDGEs simultaneously, this factor must be taken into account in the analysis of the equations.

In this paper, the servo commands  $x_{cmd}, y_{cmd},$  and  $z_{cmd}$  were used to establish the equations through inverse kinematics. When the  $C$ -axis rotates at different angles, the two variables  $C_{z(dep)}$  and  $C_{(pos)}$  will continue to change signs in the process of analyzing equations. For example,

**Fig. 8** Schematic diagram for method of establishing equations



the next angles of  $C_{z(dep)}$  and  $C_{(pos)}$  become  $C_{z(dep)2}$ ,  $C_{(pos)2}$ , and so on. The PDGE variables of each equation continue to change, but the PIGEs remain unchanged. Finally, the equations of all the measured angles of the C-axis were established and analyzed together.

### 4 Measurement method and error calculation result

#### 4.1 Measurement method and experiments

Before the experiments, a calibration process of the touch-trigger probe was executed. The calibration of the probe can ensure that this experiment is not affected by the errors of

the probe. After the calibration is completed, the operation process of measuring the coordinates of the standard calibration spheres can be started.

As stated in Sect. 2.3, two standard calibration spheres were used as the tested objects. During the experiments, firstly only the C-axis was rotated. After the C-axis was rotated to the next angle, the linear axis was used to move the touch-trigger probe to the vicinity of the calibration spheres and touch the 5 points of spheres and calculate the center coordinates of the spheres. After measuring the first sphere, the linear axis was used to move to the vicinity of the second sphere to measure its coordinates. After measuring both spheres, C-axis was rotated to the next angle. The measurement process and experimental setup are shown in Figs. 11 and 12, respectively.

**Table 4** The method of establishing equations of  $dP$

dP1	2nd position-1st ideal position
dP2	3rd position-1st ideal position
dP3	4th position-1st ideal position
...	...

#### 4.2 Method of geometric error calculation

In this section, the least squares method was used to analyze the error values through the equations introduced in Sect. 2.4. The servo command  $x_{cmd}^r$ ,  $y_{cmd}^r$ , and  $z_{cmd}^r$  of the calibration spheres with the errors when the C-axis





**Table 5** Difference between PIGEs and PDGEs

PIGEs	PDGEs
When the rotary axis rotates once, the PIGEs of each position in rotary axis are a fixed value	When the rotary axis rotates once, the PDGEs of each position are different

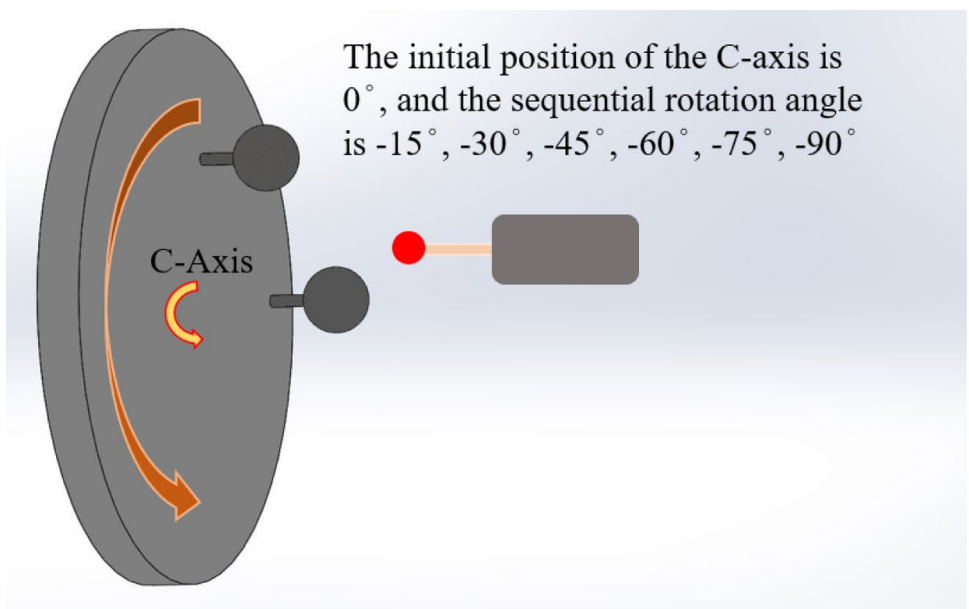
$$dP_k = \begin{bmatrix} \vdots \\ dP_{x1(\text{Ball } 1)} \\ dP_{y1(\text{Ball } 1)} \\ dP_{z1(\text{Ball } 1)} \\ dP_{x1(\text{Ball } 2)} \\ dP_{y1(\text{Ball } 2)} \\ dP_{z1(\text{Ball } 2)} \\ \vdots \end{bmatrix}_{6n} = A_{6n \times (4+2n)} E_{\text{PIGEs}+\text{PDGEs}}$$

$$= \begin{bmatrix} 1 & 0 & 0 & z_s & 0 & y_s \cos \theta_{c2} - x_s \sin \theta_{c2} & 0 & 0 & \dots & \dots \\ 0 & 1 & -z_s & 0 & 0 & -x_s \cos \theta_{c2} - y_s \sin \theta_{c2} & 0 & 0 & \dots & \dots \\ 0 & 0 & y_s \cos \theta_{c2} - x_s \sin \theta_{c2} & -x_s \cos \theta_{c2} - y_s \sin \theta_{c2} & 1 & 0 & 0 & 0 & \dots & \dots \\ \vdots & \vdots & \vdots & \vdots & \vdots & \vdots & \vdots & \vdots & \vdots & \vdots \end{bmatrix}_{6n \times (4+2n)} \begin{bmatrix} O_{xc} \\ O_{yc} \\ S_{xc} \\ S_{yc} \\ C_{z(\text{dep})1} \\ C_{(\text{pos})1} \\ C_{z(\text{dep})2} \\ C_{(\text{pos})2} \\ \vdots \\ \vdots \end{bmatrix} \tag{14}$$

The research goal is to calculate  $E_{\text{PIGEs}+\text{PDGEs}}$ . When there is a set of error values  $E_{\text{PIGEs}+\text{PDGEs}}$  that can minimize the sum of the squares of  $(dP - AE)$  in Eq. (15), that is, the

residual values, this set of values is the geometric errors of this system. Equation (15) is written in matrix form as Eq. (16).

**Fig. 11** Schematic diagram of measurement path of C-axis



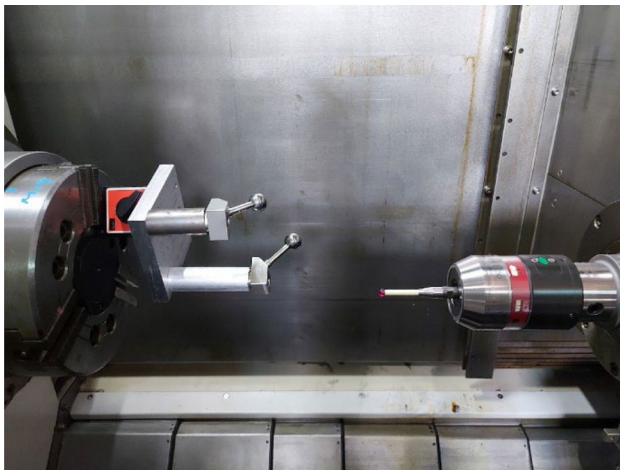


Fig. 12 Photograph of measurement process

$$Q(E_{PIGES+PDGES}) = \frac{1}{s} \sum_{s=1}^{6n} (dP - AE)^2 = \frac{1}{s} \sum_{s=1}^{6n} R_s^2 \quad (15)$$

$$\min_{PIGES} \sum_{s=1}^{6n} R_s^2 = \min_{PIGES} \left\| \begin{bmatrix} dP^1 \\ \vdots \\ dP^{6n} \end{bmatrix} - \begin{bmatrix} A_{1 \times 1} & \cdots & A_{1 \times (4+2n)} \\ \vdots & \ddots & \vdots \\ A_{6n \times 1} & \cdots & A_{6n \times (4+2n)} \end{bmatrix} \begin{bmatrix} O_{xc} \\ O_{yc} \\ S_{xc} \\ S_{yc} \\ C_{z(dep)1} \\ C_{(pos)1} \\ C_{z(dep)2} \\ C_{(pos)2} \\ \vdots \\ \vdots \end{bmatrix} \right\|^2 = \min \|dP - AE\|^2 \quad (16)$$

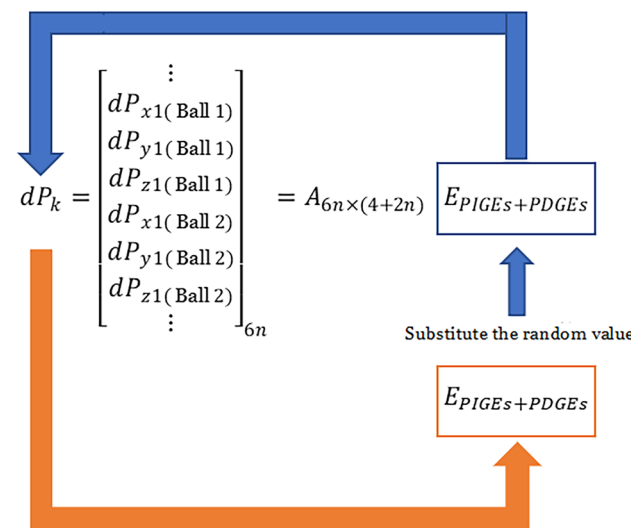


Fig. 13 Schematic diagram of error simulation

### 4.3 Simulation of calculation method

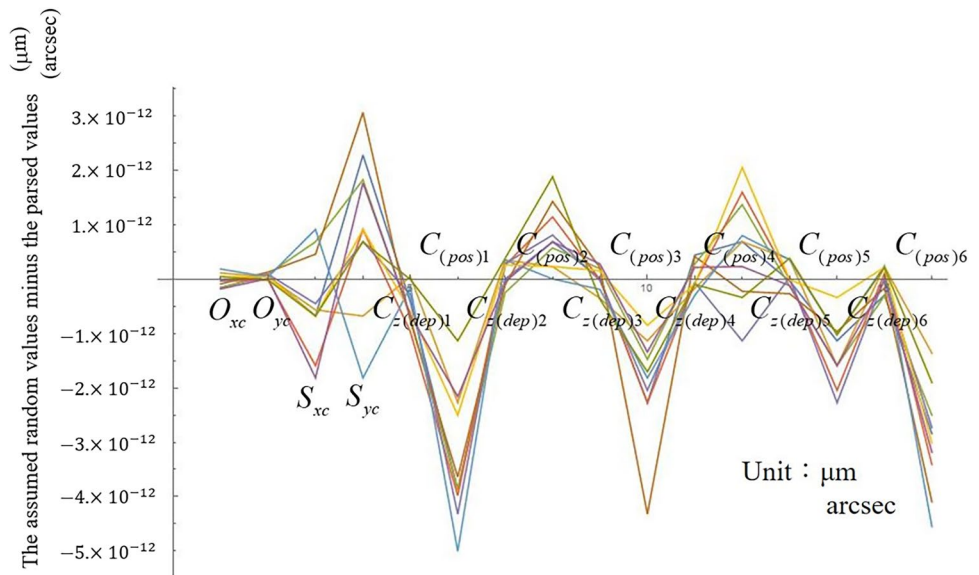
For verifying the feasibility and performance of the proposed measurement method, the simulation verification was executed through a quantitative analysis. Therefore, the main purpose of simulations is to verify the accuracy of the  $dP$  listed in Sect. 4.2, and the error values obtained by the least squares method in this section. The mathematical calculation software was used to build the simulation mode through the geometric errors model and the mathematical model which are mentioned above. Through comparing the difference between the assumed random values and the parsed values of  $dP$ , the performance of the proposed measurement method was verified.

A schematic of the process for the simulation mode is shown in Fig. 13. In the simulation mode, the analyzed error variable in the equation was substituted by a random variable. Here, the error values were regarded

as a known number. If the  $dP$  in Eq. (15) is based on experimental data, the  $dP$  was the result of subtracting the measured coordinates of standard calibration spheres. However, in the simulations, the simulated  $dP$  can be obtained without using experimental data by using random variables to substitute errors. Using the  $dP$  of the simulations and then using the least squares method resolve the error values. Following the simulation process shown in Fig. 13; the simulation results are estimated by observing the difference of the assumed random values and the parsed values. Figure 14 shows the residual values of the parsed values after deducting the assumed random values. Then,  $C_{z(dep)i}$  and  $C_{(pos)i}$  represent the axial error and angular positioning error, respectively, in the different commands for the C-axis angular positions. The index  $i$  is given as follows:

$$i = \{ -15^\circ, -30^\circ, -45^\circ, -60^\circ, -75^\circ, -90^\circ \} \quad (17)$$

**Fig. 14** Residual plot of error simulations



Furthermore, 10 independent simulations were implemented, and the results are presented in Fig. 14 by using lines of different colors. According to the simulation results, the differences between the parsed values and the assumed random values are very small, and the residual values of all geometric errors are less than  $10^{-10}$   $\mu\text{m}$  or  $10^{-10}$  arcsec. From the simulation results, it can be absolutely known that the method of synchronous analysis of PIGEs and PDGEs in this paper is accurate and feasible.

### 4.4 Measurement results

The measurement experiments were performed on a commercial mill-turn five-axis machine tool MT-540 (Yida Precision Machinery Co., Ltd.), as shown in Fig. 1. Additionally, the touch-trigger probe (type: TC50) provided by Blum-Novotest Co., Ltd. and two standard calibration spheres certified by Spheric-Trafalgar were also used for this experimental verification. As mentioned in Sects. 2.3 and 4.1, the measurement procedure was executed. First, the positions of the two standard calibration spheres were determined for the reference by using the touch-trigger

**Table 6** Error values of PIGEs

	$O_{xc}(\mu\text{m})$	$O_{yc}(\mu\text{m})$	$S_{xc}(\text{arcsec})$	$S_{yc}(\text{arcsec})$
Average	45.6046	-158.3872	-153.2539	-95.1690

probe when the position of the C-axis is at  $0^\circ$ . Moreover, the positions of the two standard calibration spheres in 6 rotation angles of the C-axis were also taken for error analysis. Based on the equations mentioned in Sect. 4.2 and the measured data of the positions of the two standard calibration spheres, the PIGEs and PDGEs of the C-axis on the five-axis machine tool were obtained. As a result, Tables 6 and 7 show the measurement results of the PIGEs and PDGEs, respectively. Among them, the measurement results shown in Tables 6 and 7 are the average of 11 pieces of data. From the measured PIGEs, the maximum linear offset and squareness errors are  $-158.3872 \mu\text{m}$  and  $-153.2539 \text{ arcsec}$ , respectively. On the other hand, for the measured PDGEs, the maximum linear and angular errors are  $-46.7580 \mu\text{m}$  and  $-204.9957 \text{ arcsec}$ , respectively. Consequently, the measurement experiments have demonstrated feasibility of this measurement system.

**Table 7** Error values of PDGEs

	$C_{z(dep)}(\mu\text{m})$ Average	$C_{(pos)}(\text{arcsec})$ Average
$0^\circ$	0.0000	0.0000
$-15^\circ$	-46.7580	-144.7235
$-30^\circ$	-43.0594	-144.8288
$-45^\circ$	-37.6213	-149.7547
$-60^\circ$	-30.2005	-164.0565
$-75^\circ$	-21.3915	-176.5736
$-90^\circ$	-11.7065	-204.9957

## 5 Conclusions

This paper has proposed the synchronous measurement method of 4 PIGEs and 2 PDGEs of the rotary axis. Compared with previous studies, PIGEs and PDGEs are usually measured separately, but these two types of errors exist in the machine tools at the same time, and the step-by-step measurement essentially ignores the other type of geometric errors. Moreover, the costly commercial measurement systems for calibrating rotary axes (e.g., *R*-test and AxiSet Check-Up) are limited only for the PIGEs of rotary axes on the five-axis machine tool. As a result, for the purpose of improving the mentioned existing disadvantages of geometric error measurement of rotary axes, the synchronous measurement system has been proposed.

Furthermore, the contributions and valuable works of this paper are depicted into several aspects as follows. For the error measurement accuracy of the machine tools, this paper considers the 4 PIGEs and 2 PDGEs of the rotary axes at the same time. In terms of convenience and economy, using the proposed measurement system to identify these two types of errors of rotary axes only needs one measurement device. For the feasibility verification, the measurement method proposed in this paper was actually applied to a five-axis machine tool. This paper also verifies the accuracy of this measurement method from the point of view of mathematical simulation. Finally, it is beneficial to perform a quick health check on PIGEs and PDGEs of rotary axes.

**Author contribution** Ting-Yu Lee: writing — original draft preparation, conceptualization, methodology, software, validation. Yu-Ta Chen: writing — reviewing and editing, methodology. Chien-Sheng Liu: writing — reviewing and editing, supervision, project administration.

**Funding** Financial support was provided to this study by the Ministry of Science and Technology of Taiwan under Grant Nos. MOST 110–2221-E-006–126-MY3, 110–2218-E-006–031, 110–2218-E-002–038, and 111–2222-E-218–001.

**Availability of data and materials** Not applicable.

**Code availability** Not applicable.

## Declarations

**Ethical approval** Not applicable.

**Consent to participate** Not applicable.

**Consent for publication** Not applicable.

**Competing interests** The authors declare no competing interests.

## References

- Chen YT, Lin WC, Liu CS (2016) Design and experimental verification of novel six-degree-of freedom geometric error measurement system for linear stage. *Opt Lasers Eng* 92
- Liu C-S, Zeng J-Y, Chen Y-T (2021) Development of positioning error measurement system based on geometric optics for long linear stage. *Int J Adv Manuf Technol* 115:2595–2606
- Gao W, Haitjema H, Fang F, Leach R, Cheung BCF, Savio E, Linares JM (2019) On-machine and in-process surface metrology for precision manufacturing. *CIRP Ann Manuf Technol*
- Liu C-C, Tsai M-S, Lin M-T, Tang P-Y (2020) Novel multi-square-pulse compensation algorithm for reducing quadrant protrusion by injecting signal with optimal waveform. *Mech Mach Theory* 150:103875
- Liu C-S, Hsu H-C, Lin Y-X (2020) Design of a six-degree-of-freedom geometric errors measurement system for a rotary axis of a machine tool. *Opt Lasers Eng* 127:105949
- Ma D, Li J, Feng Q, He Q, Ding Y, Cui J (2021) Simultaneous measurement method and error analysis of six degrees of freedom motion errors of a rotary axis based on polyhedral prism. *Appl Sci* 11:3960
- Liu C-S, Pu Y-F, Chen Y-T, Luo Y-T (2018) Design of a measurement system for simultaneously measuring six-degree-of-freedom geometric errors of a long linear stage. *Sensors* 18:3875
- Ibaraki S, Iritani T, Matsushita T (2012) Calibration of location errors of rotary axes on five-axis machine tools by on-the-machine measurement using a touch-trigger probe. *Int J Mach Tools Manuf* 58:44–53
- Liu C, Xiang S, Lu C, Wu C, Du Z, Yang J (2020) Dynamic and static error identification and separation method for three-axis CNC machine tools based on feature workpiece cutting. *Int J Adv Manuf Technol* 107:2227–2238
- Ramesh R, Mannan MA, Poo AN (2000) Error compensation in machine tools — a review: part I: geometric, cutting-force induced and fixture-dependent errors. *Int J Mach Tools Manuf* 40:1235–1256
- Tan F, Yin G, Zheng K, Wang X (2021) Thermal error prediction of machine tool spindle using segment fusion LSSVM. *Int J Adv Manuf Technol* 116:99–114
- Kiridena VSB, Ferreira PM (1994) Kinematic modeling of quasi-static errors of three-axis machining centers. *Int J Mach Tools Manuf* 34:85–100
- Shen H, Fu J, He Y, Yao X (2012) On-line asynchronous compensation methods for static/quasi-static error implemented on CNC machine tools. *Int J Mach Tools Manuf* 60:14–26
- Xiong Q, Zhou Q (2020) Development trend of NC machining accuracy control technology for aeronautical structural parts. *World Journal of. Eng Technol* 08:266–279
- Papageorgiou D, Blanke M, Niemann HH, Richter JH (2019) Adaptive and sliding mode friction-resilient machine tool positioning – cascaded control revisited. *Mech Syst Signal Process* 132:35–54
- Tan F, Yin G, Zheng K, Wang X (2021) Correction to: thermal error prediction of machine tool spindle using segment fusion LSSVM. *Int J Adv Manuf Technol* 116:115–115
- Ibaraki S, Inui H, Hong C, Nishikawa S, Shimoike M (2018) On-machine identification of rotary axis location errors under thermal influence by spindle rotation. *Precis Eng* 55
- Liu Y (2018) Identification of position independent geometric errors of rotary axes for five-axis machine tools with structural restrictions. *Robot Comput Integr Manuf* 53

19. Xiang S, Yang J, Zhang Y (2014) Using a double ball bar to identify position-independent geometric errors on the rotary axes of five-axis machine tools. *Int J Adv Manuf Technol* 70
20. Li Q, Wang W, Zhang J, Li H (2020) All position-dependent geometric error identification for rotary axes of five-axis machine tool using double ball bar. *Int J Adv Manuf Technol* 110:1351–1366
21. Chen YT, More P, Liu CS, Cheng CC (2019) Identification and compensation of position-dependent geometric errors of rotary axes on five-axis machine tools by using a touch-trigger probe and three spheres. *Int J Adv Manuf Technol* 102
22. Ibaraki S, Iritani T, Matsushita T (2013) Error map construction for rotary axes on five-axis machine tools by on-the-machine measurement using a touch-trigger probe. *Int J Mach Tools Manuf* 68:21–29
23. Jiakun L, Qibo F, Chuanchen B, Jing Y, Bintao Z (2019) Measurement method and error analysis for angular positioning error of rotary axis. *Infrared Laser Eng* 48:217001
24. Fang W, Tian X (2021) Geometric error sensitivity analysis for a 6-axis welding equipment based on Lie theory. *Int J Adv Manuf Technol* 113:1045–1056
25. Jeong JH, Khim G, Oh JS, Chung S-C (2018) Method for measuring location errors using a touch trigger probe on four-axis machine tools. *Int J Adv Manuf Technol* 99:1003–1012
26. Chen YT, More P, Liu CS (2019) Identification and verification of location errors of rotary axes on five-axis machine tools by using a touch-trigger probe and a sphere. *Int J Adv Manuf Technol* 100
27. Ibaraki S, Yoshida I, Asano T (2019) A machining test to identify rotary axis geometric errors on a five-axis machine tool with a swiveling rotary table for turning operations. *Precis Eng* 55:22–32
28. Li Z, Sato R, Shirase K, Sakamoto S (2021) Study on the influence of geometric errors in rotary axes on cubic-machining test considering the workpiece coordinate system. *Precis Eng* 71:36–46
29. Jiang Z, Tang X, Zhou X, Zheng S (2015) Machining tests for identification of location errors on five-axis machine tools with a tilting head. *Int J Adv Manuf Technol* 79:245–254
30. Viprey F, Nouira H, Lavernhe S, Tournier C (2019) Modelling and characterisation of geometric errors on 5-axis machine-tool. *Mech Ind* 20:605
31. Abbaszadeh-Mir Y, Mayer JRR, Cloutier G, Fortin C (2002) Theory and simulation for the identification of the link geometric errors for a five-axis machine tool using a telescoping magnetic ball-bar. *Int J Prod Res* 40:4781–4797
32. ISO 230–1 (2012) In Test code for machine tools —part 1: geometric accuracy of machines operating under no-load or quasi-static conditions
33. ISO 230–7 (2015) In Test code for machine tools —part 7: geometric accuracy of axes of rotation

**Publisher's note** Springer Nature remains neutral with regard to jurisdictional claims in published maps and institutional affiliations.